Photogating of ionic currents across lipid bilayers

Electrostatics of ions and dipoles inside the membrane

David C. Mauzerall and Charles M. Drain
The Rockefeller University, New York, New York 10021 USA

ABSTRACT The conductances of the lipophilic ions tetraphenylboride and tetraphenylphosphonium across a lipid bilayer can be increased or decreased, i.e., gated, by the photoformation of closed-shell metalloporphyrin cations within the bilayer. The gating can be effected by pulsed or continuous light or by chemical oxidants. At high concentrations of lipophilic anions where the dark conductance is saturated due to space charge in the bilayer, the photogated conductance can increase 15-fold. The formation of porphyrin cations allows the conductance to increase to its nonspace charge limited value. Conversely, the decrease of conductance in the light of phosphonium cations diminishes toward zero as the dark conductance becomes space charge limited. We present electrostatic models of the space charge limited conductance that accurately fit the data. One model includes an exponentially varying dielectric constant for the polar regions of the bilayer that allows an analytical solution to the electrostatic problem. The exponential variation of the dielectric constant effectively screens the potential and implies that the inside and outside of real dielectric interfaces can be electrically isolated from one another. The charge density, the distance into the membrane of the ions, about one-quarter of its thickness, and the dielectric constant at that position are determined by these models. These calculations indicate that there is insufficient porphyrin charge density to cancel the boride ion space charge and the following article proposes a novel ion chain mechanism to explain these effects. These models indicate that the positive potential arising from oriented carbonyl ester groups, previously used to explain the 10^3-fold larger conductance of hydrophobic anions over cations, is smaller than previously estimated. However, the synergistic movement of the positive choline group into the membrane can account for the large positive potential.

GLOSSARY

A_m	area of the membrane (8×10^{11} nm^2)
a	distance of the hydrophobic ion from the center of the membrane (nm)
b	distance of the counterion from the center of the membrane (nm)
β	hydrophobic ion partition coefficient (nm)
C	concentration (mol/liter)
d	inter-ion distance in the bilayer (nm), $d = (\rho_\pm)^{-0.5}$
d_m	membrane thickness (8 nm)
d_c	membrane hydrocarbon core thickness (nm)
D_{TPhB^-}	diffusion constant for $TPhB^-$ (5×10^8 nm^{2}s^{-1})
E	electric field
ϵ_0	vacuum permittivity (8.85×10^{-12} $J^{-1}C^2$m^{-1})
ϵ_1	dielectric constant for the membrane phase
ϵ_2	dielectric constant for the aqueous phase
ϵ_c	dielectric constant of the hydrocarbon core region of the membrane
F	Faraday (9.65×10^4 C mol^{-1})
G_{dk}	conductance in the dark, (S)
G_{ph}	conductance in the light, (S)
ΔG	photoconductance, $G_{ph} - G_{dk}$
h	space constant of variable dielectric
I_{dk}	current in the dark, (A)
I_{ph}	current in the light, (A)
k	Boltzmann constant (1.38×10^{-23} JK^{-1})
M	summation of the effect of lattice charges, geometry dependent
$\mu_{TPhB^-/water}$	aqueous mobility of $TPhB^-$ (2×10^{10} nm^2 s^{-1} V^{-1})
$\mu_{TPhB^-/BLM}$	mobility of $TPhB^-$ in the membrane (12 nm^2 s^{-1} V^{-1})
N	Avogadro's number (6.02×10^{23} molecules mol^{-1})
P^+	porphyrin cation
q	electronic charge (-1.60×10^{-19} C)
$\rho_\pm$	charge density of either anion or cation (nm^{-2})
ρ_{TPhB^-}	tetraphenylboride anion charge density (nm^{-2})
ρ_{TPhP^+}	tetraphenylphosphonium cation charge density (nm^{-2})
ρ_{P^+}	porphyrin cation charge density (nm^{-2})
r	$TPhB^-$ radius, 0.42 nm
S	Siemens, ohm^{-1} (Ω^{-1})
T	temperature (°K)
V	potential (volts)

Address correspondence to Dr. David C. Mauzerall, The Rockefeller University, 1230 York Avenue, New York, NY 10021.

INTRODUCTION

All metabolically active cells depend on the transport of ions across the cell membrane for their survival, and cells such as axons use ion currents for their function. Many antibiotics function by relaxing ion gradients across the cell wall via channel formation or by acting as ionophores, and some topical anesthetics are lipophilic ions (Hille, 1984). There has been a paucity of experimental or theoretical treatments of the electrostatics of mobile charges inside the bilayer lipid membrane as compared with the extensive work on the electrostatics from the bilayer-water interface into the surrounding aqueous solution. The latter subject has been well reviewed by McLaughlin (1977, 1989), by Honig et al. (1986), and by Cevc (1990). There have been earlier treatments of space charge inside the membranes (LeBlanc, 1969;

0006-3495/92/12/1544/12 $2.00

Neumcke and Lauger, 1970; Tsien and Hladky, 1982; Braun, 1987; Bender, 1988) that do not quantitatively explain data on the saturation of hydrophobic ion conductance.

The currents of negative and positive lipophilic ions such as tetraphenylboride ($TPhB^-$) and tetraphenylphosphonium ($TPhP^+$) across a lipid bilayer membrane can be gated by the photoformation of closed-shell metalloporphyrin cations within the bilayer (Drain et al., 1989). We present electrostatic models that explain both the photogating effect and the saturation of conductance with increasing lipophilic ion concentration. The models are based on the method of images in the case of a constant dielectric and on an analytical solution to the case of an exponentially varying dielectric inside lipid membranes. They allow the charge density, location, and the dielectric constant at the position of the lipophilic ions in the membrane to be quantified. These models also allow a calculation of the potential in the membrane due to the ordered dipoles of ester carbonyls or polar head groups. In addition to probing the relatively unknown electrostatic potentials within the membrane, the photogating technique affords a unique opportunity to examine the kinetics and mechanism of ions crossing the membrane that are discussed in the companion article (Drain and Mauzerall, 1992).

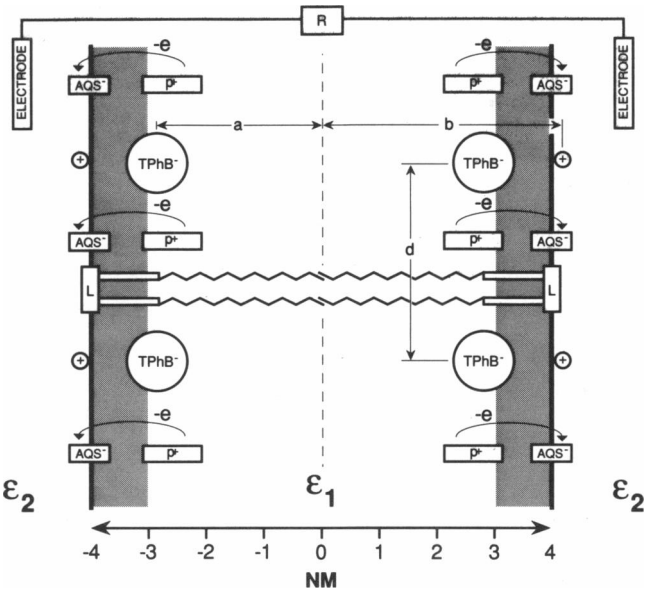

FIGURE 1 Schematic of the interfacial charge transfer and structure within the membrane. L, lipids; AQS, anthraquinone-2-sulfonate(−) the electron acceptor and + = the aqueous counter ion; $TPhB^-$, tetraphenyl boride anion; and P^+, porphyrin cation. A voltage imposed across the electrodes allows the current to be recorded at R. The relative molecular sizes are to scale, but the intermolecular distances (vertical) are condensed ~10-fold over the distances obtained at ~1 μM $TPhB^-$. The model used to estimate the electrostatic interactions includes the dielectric constants for the aqueous (ϵ_2) and membrane (ϵ_1) phases, the depth of the two-dimensional lattice of $TPhB^-$ inside the membrane (a), the distance to the lattice of counter ions in the aqueous phase (b), and the distance between ions in the membrane $d = \rho^{-1/2}$ (see Appendices 1 and 2).

METHODS

The electron donor in this system is the hydrophobic, closed-shell metalloporphyrin magnesium octaethylporphyrin (MgOEP), that is located in the polar, ester region of the lipid bilayer (Woodle and Mauzerall, 1986). A schematic representation of the porphyrin-bilayer-acceptor system is presented in Fig. 1. The charged electron acceptor is restricted to the aqueous phase or to the membrane-water interface and is chosen to have the same sign of charge as the hydrophobic ion to avoid ion pairing and charge transfer complex formation. In these experiments, 15–20 mM methylviologen(+2) is the electron acceptor when $TPhP^+$ is the lipophilic ion, and 0.1–0.5 mM anthraquinone-2-sulfonate(−1) is used with $TPhB^-$. These concentrations are above those needed to saturate the photovoltage (Ilani and Mauzerall, 1981). The membrane is formed in a 1-mm^2 aperture in a 0.38-mm-thick Teflon divider in a 4-ml polyethylene cell with glass windows, from a solution composed of 3.2% (wt/vol) diphytanoylphosphatidylcholine and 3.6 mM MgOEP in decane across symmetrical 1 mM, 100 mM, or 1 M NaCl solutions containing 0.1 mM, 10 mM, or 10 mM *N*-2-hydroxyethylpiperazine-*N'*-2-ethane sulfonic acid (Hepes) buffer (pH 7.1), respectively. Fresh stock solutions of $TPhP^+$ chloride or sodium $TPhB^-$ in 1:1 ethanol/water (vol/vol) and the appropriate electron accepter in water are added to each side of the membrane after it has formed. The ethanol content in the bathing solutions never exceeded 1% by volume and typically is kept below 0.5% to minimize any effect of this solvent on the membrane (Andersen et al., 1976). The area of the membrane is $\sim 8.0 \times 10^{11}$ nm^2 when the annulus is ~10% of the radius. The membrane thickness, as measured by its capacitance (5 nF) before the addition of lipophilic ions or electron accepters, varies by < ±10%. This yields a hydrocarbon core thickness of ~3 nm, assuming the dielectric constant of the hydrocarbon core of the bilayer is 2.5. Lipids are from Avanti Polar Lipids, Inc. (Pelham, AL) and the porphyrins are from Aldrich Chemical Co. (Milwaukee, WI) or from Porphyrin Products (Salt Lake City, UT). $TPhB^-$ from K & K Labs (Plainview, NY) and $TPhP^+$ from Fluka (Buchs, Switzerland) are recrystallized from 95% ethanol before use. All other chemicals are analytical grade and used without further purification. The experiments are at room temperature that is maintained at 22 ± 2°C.

The light pulse is from a SLL-250 flash-lamp (Candela Laser Corp., Wayland, MA) pumped dye laser, 1 μs (FWHM) at 596 nm, and 1–2 mJ maximum energy after passing through a 1 OD neutral density filter as measured by a Laser Precision Corp. Rj-7200 energy meter. The current is measured by two calomel electrodes with saturated KCl bridges immersed in the bathing solutions on each side of the membrane and monitored by a homemade fast operational amplifier (model 1021; Teledyne Philbrick, Dedham, MA) with a feedback loop of adjustable gain and time constant. The current in the dark (I_{dk}) and the current in the light (I_{ph}) are divided by the applied voltage to obtain the conductance in the dark (G_{dk}) and the conductance in the light (G_{ph}). To maintain the symmetry of the system and to avoid polarizing the membrane, a ± square wave voltage (0–150 mV) is applied for 1–100 s across the membrane by a homemade voltage source. The data are corrected for a 3-mV asymmetry in the electrodes and a 25-pS leakage conductance. The laser pulse is set to trigger ~1 s after the membrane capacitative transient, which decays more slowly with increasing hydrophobic ion concentration (Andersen and Fuchs, 1975). At $TPhB^-$ concentrations < 10^{-7} M, the system is allowed to reach equilibrium for ~5 min between laser pulses with the continued application of the square wave voltage. A large Faraday cage surrounds the battery-powered amplifier and voltage source, and a smaller Faraday cage contains the polyethylene cell and the electrodes. The entire assembly rests on a vibration absorbing base. Typically, the operational amplifier is set at 10^7–10^8 V/A with a time constant of 0.1–1 ms, and unless otherwise noted a ±40-mV square wave is applied across the

membrane and a saturating light pulse is used. The signal is digitized by means of a high-speed voltmeter (model 194; Keithley Instruments, Cleveland, OH) and stored in a computer (model 318; Hewlett-Packard Co., Palo Alto, CA). The current is continuously monitored by a Biomation transient recorder (model 802; Gould Instruments, Inc., Valley View, OH). Both positive and negative applied voltages are used, but for maximum figure clarity, the absolute value of the current and voltages are plotted. The photovoltages are measured with a differential voltmeter, (model 560; Stanford Research Instruments, Sunnyvale, CA), $10^8\Omega$ input impedance.

All the data shown are from an average of at least three different membranes that each average 8–16 laser pulses for currents below 10 pA and 4–8 laser pulses for currents above 10 pA. Typically, one membrane is used to investigate only three to four concentrations of hydrophobic ion to minimize the amount of ethanol present in the bathing solutions. The $TPhB^-$ data in 0.1 M NaCl is the average of measurements on at least five membranes. Since the lipophilic ions can stick to the cell, it is washed four to five times with water, four to five times with 95% ethanol, sonicated for ~15 min in ~50% ethanol in chloroform (vol/vol), rinsed with water, and soaked overnight in 95% ethanol.

RESULTS

At low lipophilic ion concentrations where G_{dk} increases linearly with increasing concentration, the photoformation of $MgOEP^+$ in the bilayer with a saturating light pulse causes the conductance of $TPhB^-$ ions to transiently increase 30–50% and the conductance of $TPhP^+$ to transiently decrease 20–30% (Drain et al., 1989). At high concentrations of $TPhB^-$ where G_{dk} saturates with increasing concentration of this lipophilic ion, the conductance increases up to 15-fold on photoformation of $MgOEP^+$. The maximum in the time course of the light-initiated conductance minus the dark conductance is referred to as the photoconductance (ΔG). (Examples of the current versus time traces at high concentrations of $TPhB^-$ are to be found in Fig. 1 of the companion article Drain and Mauzerall (1992)). The conductances versus $TPhB^-$ concentration are illustrated in Fig. 2 *A–C*. The G_{dk} (*closed circles*) shows a slow saturation with increasing concentrations of $TPhB^-$, whereas the G_{ph} (*open circles*) remains approximately linear. A similar saturation of G_{dk} is observed for $TPhP^+$, but G_{ph} decreases to zero as the concentration of this ion increases (Fig. 2 *D*). The solid lines in these figures represent the best fit of the electrostatic models to the G_{dk} data, whereas the dashed line represents the nonspace charge limited conductance, vide infra, and the G_{ph} data are close to these lines.

The ionic strength of the membrane bathing solutions has a strong effect on β, the distribution of lipophilic ions into the membrane, but has little effect on the dark or photo conductances. At 1 mM NaCl (Fig. 2 *A*), the linear conductance of 0.1 nS is observed at 4 nM $TPhB^-$, whereas at 100 mM (Fig. 2 *B*) and 1 M NaCl (Fig. 2 *C*), this conductance occurs at 30 and 20 nM $TPhB^-$, respectively.

When the photogating system containing 2 μM $TPhB^-$ is irradiated with nonsaturating, continuous, white light, the photogating signal is 75% of the maximal pulsed photosignal and decreases by only 10–15% over the next 20 min if the solution is vigorously stirred (Fig. 1 *B* of Drain and Mauzerall, 1992). This process is repeatable for the lifetime of the membrane. If the solutions are not stirred during this experiment, G_{ph} decreases to ~G_{dk} within 2 min. When the porphyrin is oxidized with potassium hexachloroiridate (IV) in the dark, the conductance increases to ~90% of the maximal $\Delta G/G_{dk}$ value obtained on laser irradiation and lasts 30–50 s, depending on the concentration of the oxidant. After the signal has decayed, the addition of more chemical oxidant results in a similar signal, and this can be repeated five times without significant decay in the maximal chemically gated signal. Removing dioxygen with a glucose/glucose oxidase/catalase system (Ilani et al., 1985) has less than a 5% effect on the magnitude of the photogating signal and no measurable effect on G_{dk}.

Results similar to the MgOEP data are obtained with zinc tetraphenylporphyrin. However, when zinc protoporphyrin IX (2 carboxylate groups) is used as the electron donor, the photogating effect under the same conditions (3.33 μM $TPhB^-$ and 100 mM NaCl) is only 25% of the MgOEP value. No photogating effect, $\Delta G/G_{dk} <$ 3%, is observed when zinc coproporphyrin I (4 carboxylate groups) is used as the electron donor. The photovoltages observed when using these porphyrins are also smaller or not detectable (Ogawa and Mauzerall, 1988).

The following discussion focuses primarily on the $TPhB^-$ system because of the amount of published work on this ion, but photogating is observed with other hydrophobic anions such as carbonylcyanide-3-chlorophenylhydrazone. The inverse system also applies since the anaerobic generation of the porphyrin anion using ascorbate as the reductant causes an increase in $TPhP^+$ currents and a decrease in $TPhB^-$ currents (Drain, C. M., and D. C. Mauzerall, unpublished experiments).

Electrostatic models

Electric charges on membrane surfaces are often discussed as distributed sheets of charge. In a constant dielectric, the space between the two sheets of opposite charge will have a linearly varying potential (V) and a constant electric field (E), whereas the potential outside is constant and the field is zero (Jackson, 1975). However, for real lattices of ions with separation of the order of the membrane thickness, such an assumption of continuous charge is misleading. The lattice inter-ion distance cannot be duplicated by a smeared surface charge since now the potentials and the fields change both inside and outside the space enclosed by the charges and depend on the inter-ion separation. For similar reasons, calculations with finite dipoles are needed since the point dipole model collapses the change of sign of the potential to a point or a surface.

The question of single ion and dipole potentials inside a lipid bilayer have been discussed (Neumcke and Lauger, 1969; Flewelling and Hubbell, 1986*b*). However, the membrane potential in the presence of numer-

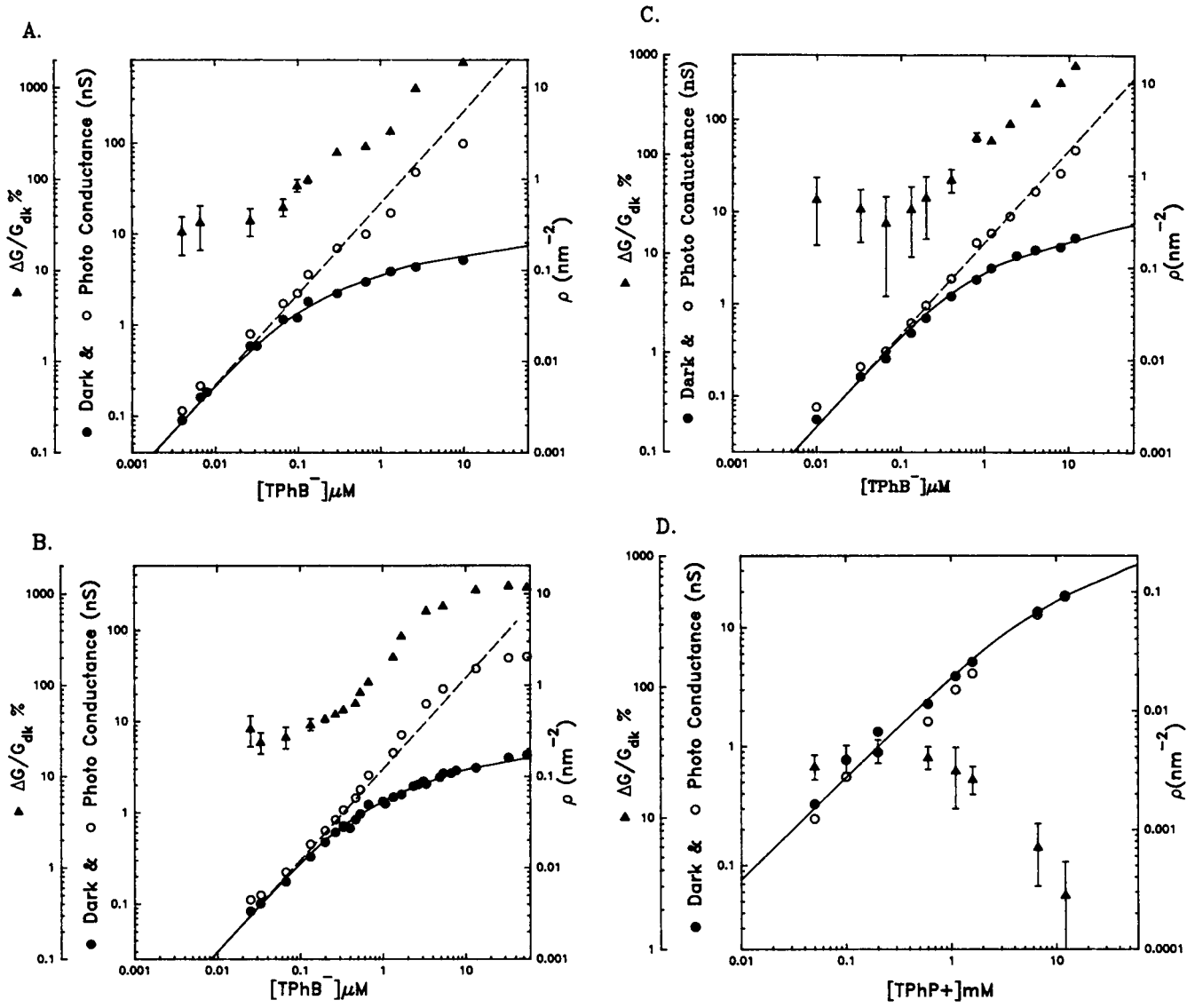

FIGURE 2 Log-log plots of the experimental conductance and the calculated charge density as a function of concentration of $TPhB^-$ and $TPhP^+$. The solid line is the fit of the implicit Eq. 1 to the experimental data for the dark conductance of the hydrophobic ions. The dashed line represents the non-space-charge-limited conductance of the hydrophobic ion. The filled circles represent the dark conductance, whereas the open circles represent the conductance maximum for $TPhB^-$ and minimum for $TPhP^+$ on photocharging the membrane. Each $TPhB^-$ experiment is at ±40 mV, whereas the $TPhP^+$ experiment is at ±50 mV and the light pulse is saturating in each. The filled triangles are a plot of $\Delta G/G_{dk}$% versus the hydrophobic ion concentration that uses the left, outside axis. Note the standard deviation of the G values increases slowly with decreasing conductance and on this log-log scale is smaller than the symbol size, but these errors are amplified in the plot of $\Delta G/G_{dk}$, where the root mean square of the errors are plotted. The parameters used to fit the data are listed in Table 1. (*A*) $TPhB^-$, 1 mM NaCl. (*B*) $TPhB^-$, 100 mM NaCl. The steady-state G_{dk} above ~10 μM varies by ±20% due to destabilization of the membrane by $TPhB^-$ (*C*) $TPhB^-$, 1 M NaCl. (*D*) $TPhP^+$, 100 mM NaCl.

ous hydrophobic ions, or space charge effect, has been treated only cursorily (LeBlanc, 1969; Parsegian, 1969; Neumcke and Lauger, 1970; Tsien and Hladky, 1982; Kleijn and Bruner, 1983). This is because of the inherent complexity of this many-body problem. We have chosen a simple rigid lattice approach to make the problem tractable. The balance of hydrophobic and electrostatic energies tends to restrict hydrophobic ions to a two-dimensional layer inside the lipid membrane, and inter-ion repulsion will favor a simple lattice, such that the inter-ion distance becomes more defined as the density of ions increases.

Two calculations were developed for the potentials inside a bilayer caused by lattices of opposite charges. The first models the membrane as a homogeneous dielectric layer with a dielectric constant less than that of water but greater than that of hydrocarbon. The second incorporates a more realistic variable dielectric constant in the membrane that decreases exponentially from the bilayer-water interface to the center of the membrane and

then increases to the opposite interface symmetrically. Both of these calculations are based on exact solutions to the electrostatic problem.

In the first, two-dielectric model, a square lattice of charges at a given distance inside the bilayer parallel to the membrane-water interface is balanced by an in-register lattice of counter charges at a second distance in the higher dielectric medium (Fig. 1). A square lattice was chosen for simplicity and because the energetics are similar to that of the hexagonal lattice (Topping, 1927). The potential inside the membrane for a simple ion pair is computed by the method of images (Harnwell, 1949). The potential of a large number of these ion pairs is summed to obtain the potential of an infinite lattice. A $\sim 200 \times 200$ lattice is within 1% of the infinite value. This summation produces a two-dimensional analogue of the Madelung constant, ~9 (Topping, 1927), which can be much larger than that found in three-dimensional lattices, ~2. The potential is calculated along an ion pair axis perpendicular to the membrane surface. This axis is chosen because it is the minimal energy axis along which an ion (a lattice ion) can move across the plane of the lattice. An ion moving through the center of the square lattice of ions will see a potential that is greater than that at a site. The exact factor depends on the charge density, $\rho_{\pm}$, and is model dependent. Thus, our calculation minimizes the electrostatic potential in a bilayer. The (self) potential from the ion pair on axis is omitted since the resulting energy is already included in the dilute binding constant, β. Neumcke and Lauger (1969) accounted for the finite thickness of the bilayer by using an infinite series of reflected images. Since our system is symmetrical in distribution of ions, and thus ionic potential across the membrane, we can obtain the actual potential by reflecting that calculated for the first half. In this two-dielectric model, this reflection doubles the calculated potential. The applied voltage disturbs this symmetry but the linearity of the current versus voltage indicates the effect is small. The algorithm is given in Appendix 1. A plot of the resulting potential from an array of negative charges 1.6 nm inside the lower dielectric (2.4 nm from the center) with the counter ions on the surface at a charge density sufficient to cause a 50% saturation of $G_{\text{TPhB}-}$ is shown in Fig. 3. The parameters are given in Table 1. A crucial aspect of this calculation is that the dielectric constant of the lower dielectric is decreased with the depth of the lattice into the membrane following an exponential relation (see below).

The most notable feature of the potential profile calculated by this two-dielectric model is the extended region inside the membrane where the potential continues to increase, well beyond the position of the ionic lattice. The spatial constant of the increase is a function of the charge density, becoming infinitely small only as the charge density approaches infinity. Thus, unlike the smeared charge models, the discrete charge model indicates an extensive electric field (potential gradient) outside the sandwich of the charged lattices. This is a more realistic potential profile because of the use of discrete charged pairs rather than point dipoles or smeared charges. The important variables are the depth of the charge in the membrane from the surface, $e = a - (d_m/2)$, where d_m is the thickness of the membrane, a the distance from the center, and ϵ_1 the membrane dielectric constant. At a given charge density, the potential is largely determined by the ratio e^2/ϵ_1. Thus, to determine e in this model, it is assumed that the dielectric constant is an exponential function of distance inside the real membrane, and this value is used as ϵ_1. The exponentially varying dielectric is justified below.

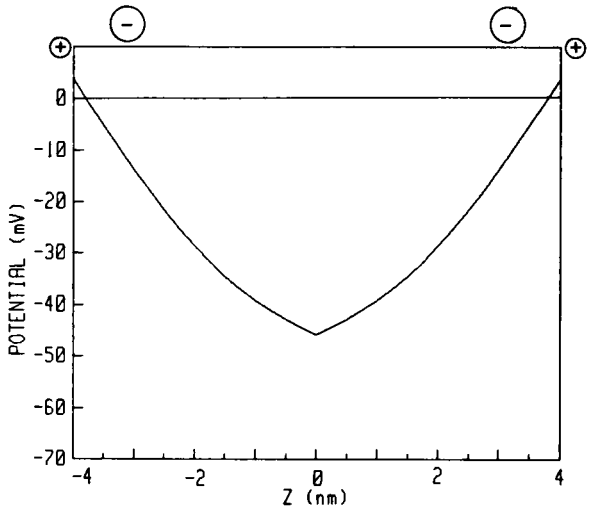

FIGURE 3 The membrane potential resulting from lattices of $TPhB^-$ and counter ions on both sides of the membrane using the two-dielectric model. The total potential results from multiplying the potential of a lattice on one side of the membrane by two and reflecting this profile through the plane at the center of the membrane. This model assumes the membrane is a homogeneous dielectric, ϵ_1, adjacent to an aqueous phase, $\epsilon_2 = 80$. The parameters used in the calculation are close to those used to fit the 0.1 M NaCl $TPhB^-$ data at $\Delta G/G_{dk} = 1$ (Table 1). They are $\rho_{\text{TPhB}^-} = 0.05\ \text{nm}^{-2}$, (Fig. 2 *B*), $a = \pm 2.4$ nm, $b = \pm 4$ nm, and the value of $\epsilon_1 = 20$ is taken from the dielectric profile for the exponential-dielectric model (Fig. 4 *A*). The circled + and − denote the position of the ion lattices.

There is general agreement that in addition to the interfacial head group region of the lipid bilayer-water system, there exists a polar region in the lipid where the fatty acids are esterified to the glycerol and that this polar region is partially penetrated by water molecules (Simon and McIntosh, 1986). Thus, a model membrane having a variable dielectric "constant" progressing from 80 in the water to ~3 in the hydrocarbon core region of the bilayer is more realistic and has been heuristically modelled by Flewelling and Hubbell (1986*b*). In a calculation of the dielectric constant of the phosphatidylcholine head group region of the bilayer, Raudino and Mauzerall (1986) estimated $\epsilon\perp \simeq 25$ and $\epsilon\parallel$ varies from $\simeq 15$ to 500 from the crystalline to the fluid case. It was also noted that an analytical solution to the fundamental equations

TABLE 1 **Model parameters used to fit the data in Fig. 2**

Experiment (Fig.)	$\rho_{\pm}$	β	Two dielectric		Exponentially variable dielectric	Exponential core model
			ϵ_1	a	a	a
	nm^{-2}	nm		nm	nm	nm
MgOEP/TPhB$^-$						
1 mM NaCl (2 *A*)	0.04	9×10^5	23	2.6	1.8	1.7
0.1 M NaCl (2 *B*)	0.05	2×10^5	27	2.8	2.1	2.0
1 M NaCl (2 *C*)	0.08	3×10^5	30	2.9	2.4	2.6
MgOEP/TPhP$^+$						
0.1 M NaCl (2 *D*)	0.06	85	21	2.5	1.8	1.7

The parameters used to fit the two-dielectric, exponentially variable dielectric, and exponential core models to the data. The value of ϵ_1 in the two-dielectric model is assumed to be that calculated at the charge depth a by the exponential variation with distance of the exponential-dielectric model. The value for a is from the center of an 8-nm membrane (see Fig. 1). The core for the exponential-core model extended to 1.5 nm, i.e., total core of 3 nm. The charge densities are taken from Fig. 2 at the point where $\Delta G/G_{dk} = 1$ and the potential calculated from Eq. 1 is ~17 mV. The error in a is ±10%. The value of β in 0.1 M NaCl is taken from Flewelling and Hubbell (1986*a*).

of electrostatics can be obtained for an exponential variation of ϵ along a single axis in a planar or spherical system. The calculation is given in Appendix 2. Note that the result (Eq. A2-4) is a screened (by the variable dielectric!) Coulomb potential, quite analogous to the Debye–Huekel potential.

Again, an array of positive and negative charges in aligned lattices are summed to obtain the potential at a given point (Appendix 2). The simplest model for the bilayer dielectric is an exponential, decreasing from ϵ = 80 at the interface to $\epsilon \sim 3$ in the hydrocarbon core and a symmetric rise to the other interface (Fig. 4 *A*). The contribution from the bulk water is neglected because it is small (Raudino and Mauzerall, 1986) but can be approximated as with the core (see below). The spatial exponential dependence of the dielectric can be viewed as a time and space average of the fluctuations of the lipid molecules and of penetration by water. This model now has only one parameter, the distance of the charge from the center of the membrane, assuming the counter ion is on the surface of the bilayer. The dielectric space parameter (h, Eq. A2-2) is defined by the thickness of the membrane and the dielectric constants of the water (80) and the hydrocarbon core (3). The calculated potential is not sensitive to small variations in these numbers. The dielectric profile is shown in Fig. 4 *A*, and the resulting potential profile for $\Delta G/G_{dk} = 1$ is shown in Fig. 4 *B*. Because the charges are more shielded, the hydrophobic ions must be placed deeper inside the membrane than with the two-dielectric model to fit the saturation of G_{TPhB^-} (Table 1).

This simple model minimizes (to zero) the core region of the membrane. A constant dielectric core of ϵ_c can be added at the center of the membrane, and the electrostatic problem solved approximately, as shown in Appendix 2. The result is a more customary dielectric profile (Fig. 5 *A*) and is referred to as the exponential-core model. The potential profile is shown in Fig. 5 *B*. The

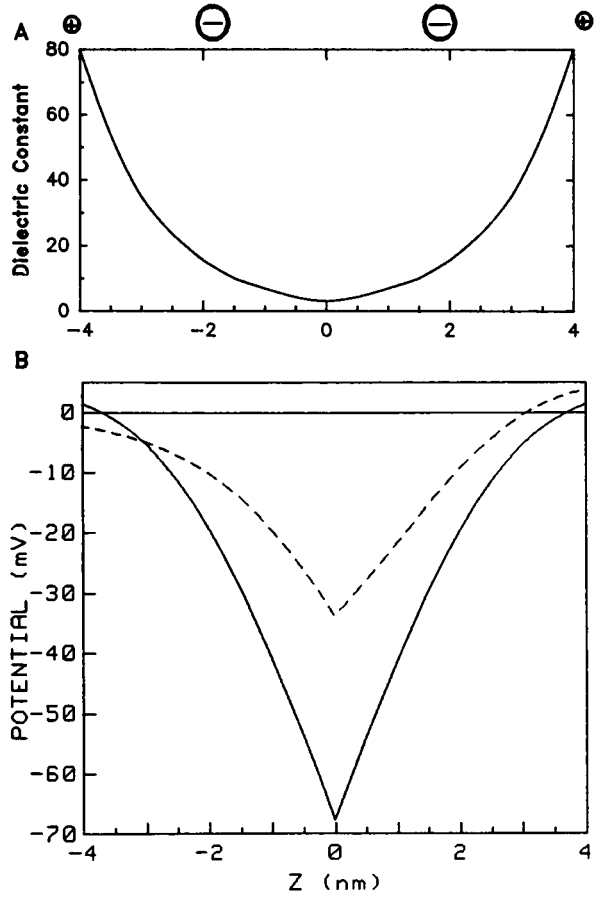

FIGURE 4 (*A*) The membrane dielectric constant profile for the exponential-dielectric model that assumes the dielectric constant is exponentially dependent on distance from the center (Eq. A2-2). (*B*) The membrane potential profile resulting from lattices of TPhB$^-$ and counter ions on both sides of the membrane using the exponential-dielectric model (*solid line*). This is the summation of the contributions from each lattice, one of which is shown as the dashed line. The parameters used in the exponential-dielectric calculation are those used to fit the 0.1 M NaCl TPhB$^-$ data at $\Delta G/G_{dk} = 1$ (Table 1). In this case, $\rho_{TPhB^-} = 0.05$ nm^{-2} (Fig. 2 *B*), $a = \pm 2.1$ nm, $b = \pm 4$ nm.

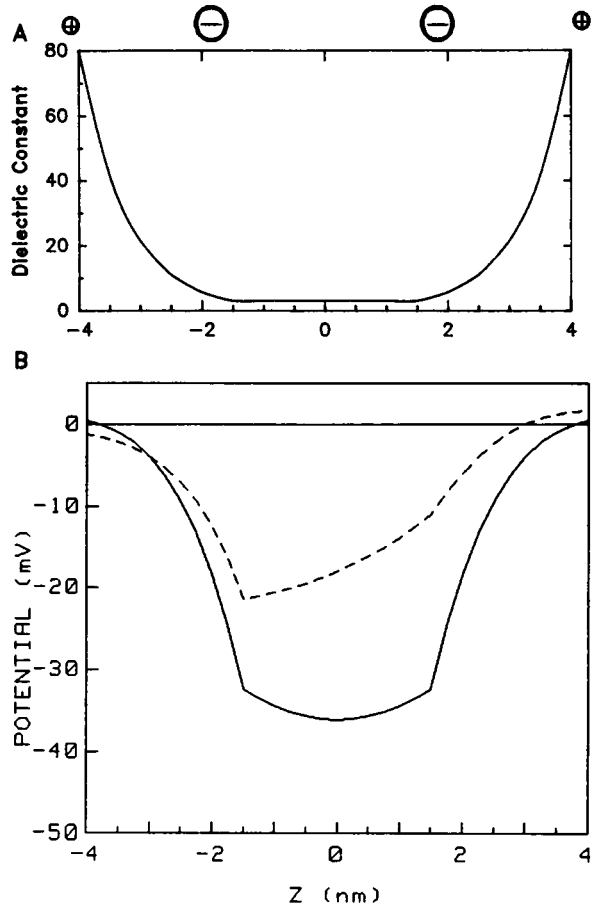

FIGURE 5 (*A*) The membrane dielectric constant profile for the exponential-core model. A hydrocarbon core region is inserted between the two regions of exponentially decreasing and increasing dielectric constants. (*B*) The membrane potential profile resulting from lattices of $TPhB^-$ on both sides of the membrane using the exponential-core model (*solid line*). This is the summation of the contributions from each lattice, one of which is shown as the dashed line. The parameters used in this are $\rho_{TPhB^-} = 0.05\ nm^{-2}$ (Fig. 2 *B*), $a = \pm 1.9$ nm, $b = \pm 4$ nm, and the core region extends over ± 1.5 nm.

calculated potentials decrease as h increases, but the ion positions are not much affected by a core size of 3 nm (Table 1). This is a reflection of the screening of the charge by the distance-varying dielectric.

DISCUSSION

Several important features of this molecular photogating system include the following: (*a*) the self-organizing design of this interfacial system ensures separation of charge on photoexcitation of the porphyrin; (*b*) the vectorial charge transfer has a quantum yield of ~0.1 (Hong and Mauzerall, 1976) and can occur in <5 ns (Woodle et al., 1987); (*c*) the porphyrin cation is relatively immobile, requiring >0.1 s to cross the bilayer (Woodle and Mauzerall, 1986); (*d*) the lifetime of the porphyrin cation is several seconds but can be shortened to μs by the addition of aqueous electron donors (Hong and Mauzerall, 1976); and (*e*) there are minimal capacitative transients generated on photocharging the membrane because of the symmetry of the system (Drain et al., 1989). The applied voltage removes this symmetry and allows small transients to be seen, particularly with substituted aryl borides (Sun, K., and D. C. Mauzerall, unpublished data). The half-wave oxidation potential of $TPhB^-$ is 0.92 V in acetonitrile (Geske, 1959), and the oxidizing potential of $MgOEP^+$ is 0.77 V *in the bilayer* (Ilani and Mauzerall, 1981), both versus the standard hydrogen electrode. Thus, only minor redox chemistry between these two species is expected. This may be observed at very low $TPhB^-$ concentrations where readdition of this ion is required to observe the same magnitude of photogating after several light pulses. Likewise, electron transfer between photoexcited magnesium porphyrin and $TPhB^-$ is negligible, since no change in photovoltage was observed in unsymmetrical acceptor experiments in the presence of the hydrophobic anion.

Saturation of conductance

Space charge limited currents of $TPhB^-$ are observed when the charge density of the hydrophobic ions inhibits further negative ions from binding to the membrane. (LeBlanc, 1969; Neumcke and Lauger 1970; McLaughlin, 1977; Andersen et al., 1978). An implicit Eq. 1 describes the saturation of lipophilic ion charge density, $\rho_\pm = \rho_{TPhB^-}$ or ρ_{TPhP^+}, inside the membrane:

$$\rho_\pm = 0.602 C \beta \exp(-qV_{\rho_\pm}), \qquad (1)$$

where C is the concentration of the lipophilic ion in the aqueous phase, β is the partition coefficient, q is the charge, and V the potential at the depth of the ion that is calculated by one of the three electrostatic models. The factor 0.602 converts units of concentration (mol $liter^{-1}$) to ions per nm^3. For comparison with measurement, one must relate the conductance of the lipophilic ion-membrane system to $\rho_\pm$. The simplest assumption is a direct proportionality via a mobility, μ:

$$G = q\mu\rho_\pm A_m / d_m^2, \qquad (2)$$

where A_m is the area of the membrane and d_m its thickness. This implies that the mobility is independent of $\rho_\pm$. Further discussion of this assumption will be given in the companion article (Drain and Mauzerall, 1992). The electrostatic calculation of V for Eq. 1 can be found in the appendices. The value of β was taken from Flewelling and Hubbell (1986*a*). The solid lines in Fig. 2 are fits of Eq. 1 (via Eq. 2) to the G_{dk} data with either the two dielectric or the exponential-dielectric models.

The parameters used for each model to fit the saturation data are given in Table 1. Note that we use the potential at the depth of the hydrophobic ion since this is the potential relevant to the electrostatic energy term in Eq. 1. This depth, ~2 nm for an 8-nm bilayer, is in full agreement with NMR measurements (Ellena et al., 1987; Smith et al., 1992), which in turn disagree with the essentially surface binding of previous electrostatic mod-

els (Tsien and Hladky, 1982; Flewelling and Hubbell, 1986*b*). The charge density calculated with our models in 100 mM NaCl, $\rho_{TPhB^-} = 0.07$ nm^{-2} at 1 μM $TPhB^-$, agrees remarkably well with the charge density obtained from experiments examining the capacitative transient after an applied voltage pulse, 0.06 nm^{-2} (Andersen et al., 1978). Flewelling and Hubbell (1986*b*) report that G_{dk} begins to saturate when $\rho_{TPhB^-} = 0.05$ nm^{-2}, and in our system G_{dk} is at one-half its linearized value at $\rho_{TPhB^-} = 0.05$ nm^{-2}.

The counter ions in the aqueous phase could be placed at the Debye length from the bilayer-water interface, ~1 nm in 0.1 M salt. Calculations using the exponential-dielectric model indicate the surface potential is $\sim kT$ when $\rho_\pm$ is ~0.05 nm^{-2}. These calculations also indicate that the location of b between 0 and 2 nm from the membrane surface in the aqueous solution has only a small effect on the surface and membrane potentials when $\rho_\pm < 0.05$ nm^{-2}, but the value of b makes important contributions to the inner membrane potential at $\rho_\pm$ greater than this. Thus, to conservatively minimize the potentials at high charge densities, we chose to place the counter ions at the surface of the membrane ($b = 4$ nm).

The partition coefficient β term has the unit of length and is equal to the thickness of the aqueous solution layer containing the same amount of hydrophobic ions as that bound to the membrane. It depends both on the type of lipid and on the ionic strength of the bathing solution (Lauger et al., 1981; Flewelling and Hubbell, 1986*a*). $TPhB^-$ and $TPhP^+$ ions have been shown to be nonideal solutes, and the activity coefficients have been estimated by solubility and spin probe effects (Flewelling and Hubbell, 1986*a*, *b*). As the ionic strength increases from 0.001 through 1, the value of β decreases from 9×10^5 nm to a minimum at 2×10^5 nm at an ionic strength of 0.1 and then increases to 3×10^5 nm, whereas the value of a, the hydrophobic ion binding position is relatively unaffected (Table 1). Our estimates of the relative activity coefficients from solubility data in 1 mM, 0.1 M, and 1.0 M NaCl are 3, 0.8, and 1.5, respectively, showing that β is proportional to these activity coefficients.

Photogating

An estimate of the minimum charge density of the porphyrin cation in the membrane, ρ_{P^+}, can be made from the observed photovoltage, 5 mV on 5 nF of $A_m = 8 \times 10^{11}$ nm^2. It is 2×10^{-4} nm^{-2}, in which case the photogating electrostatic effects would be negligible. However, the charge of the porphyrin cation acceptor anion pair is across the polar region of the bilayer (Hong and Mauzerall, 1976), $\epsilon = 25$, thickness $l \simeq 1$ nm, not the measured charge across the hydrocarbon core, $\epsilon = 2.5$, $l \sim 4$ nm. Thus, the photogenerated charge is some 40 times that measured, $\rho_{P^+} \sim 8 \times 10^{-3}$ nm^{-2} (Drain et al., 1989).[1]

[1] In this reference, the charge density had units of nm^{-3} and we had assumed a 1-nm depth of the ions inside the membrane.

The maximum ρ_{P^+} can be calculated from the ratio of MgOEP to lipid in the membrane forming solution with the unlikely assumptions that the same ratio remains in the bilayer and that all the porphyrin is converted to the cation by the saturating 1-μs laser flash. This upper bound for ρ_{P^+} is 0.1 nm^{-2}. It is known that in the case of chlorophyll, ~10% of the original chlorophyll appears in the bilayer (Cherry et al., 1972). Thus, these estimates yield a ρ_{P^+} of $\sim 10^{-2}$ nm^{-2}.

Since V depends not only on ρ_{TPhB^-} but on the distance into the membrane and the dielectric constant at this position, one can gain some of the missing potential by placing the $MgOEP^+$ ions deeper into the membrane than the $TPhB^-$ ions. However, to be consistent, the amount of charge estimated by the capacitator model should be decreased because of the decrease in the ratio of the dielectric constant to the capacitator thickness ϵ/l. If the maximum ρ_{P^+} is taken to be 8×10^{-3} nm^{-2} and the porphyrin lattice is at the same location of the $TPhB^-$ lattice, $a = 2.4$ nm from the center, then the potential caused by the porphyrin lattice is ~2 mV using the two-dielectric model. If the porphyrin lattice is moved 1-nm deeper inside the membrane, the potential at the $TPhB^-$ depth is ~14 mV or somewhat less than that of the $TPhB^-$ lattice when $\rho_{TPhB^-} = 0.05$ nm^{-2}. Calculations with the exponential-dielectric models also show that the porphyrin cation lattice cannot cancel all of the lipophilic ion space charge at realistic charge densities and locations in the lipid bilayer. The conduction mechanism will be explored in detail in the companion article (Drain and Mauzerall, 1992) where we will provide a second estimation of ρ_{P^+} with the same result.

The electrostatic models predict that the magnitude of the photogating effect will be sensitive to the position of the porphyrin cation within the bilayer. Polar porphyrins partition into the membrane closer to the water interface (Ricchelli et al., 1991) where distance a is increased and ϵ_1 is increased. This will decrease the photogenerated potential, resulting in a smaller photogating effect. The observed fourfold smaller photogating with protoporphyrin IX (−2 charge) and the lack of effect with coproporphyrin I (−4 charge) results are consistent with these expectations and are in agreement with the observation of smaller photovoltages (Ogawa and Mauzerall, 1988) with these porphyrins than with MgOEP. However, the results are qualitative because the amounts of porphyrin cations formed may vary.

Mobility and barriers

The mobility of $TPhB^-$ in the membrane ($\mu_{TPhB^-/BLM}$) is an important parameter when considering the G_{dk} and G_{ph} of the bilayer system. Given the G_{dk} of 0.25 nS in the low concentration regime (10^{-7} M $TPhB^-$, 0.1 M NaCl), the charge density of the lipophilic ions ($\rho_{TPhB^-} = 0.01$ nm^{-2}), estimates of the bilayer thickness ($d_m = 8$ nm), and its area $A_m = (8 \times 10^{11}$ nm^2), one can estimate

the bulk mobility, $\mu_{TPhB^-/BLM} \simeq G_{dk} d_m^2 / q\rho_{TPhB^-} A_m \simeq 12$ $nm^2 s^{-1} V^{-1}$. The mobility of $TPhB^-$ in water is 2×10^{10} $nm^2\ s^{-1} V^{-1}$ (Skinner and Fuoss, 1964), which is the same value as obtained from the diffusion constant of $5 \times 10^8\ nm^2\ s^{-1}$ calculated by the Stokes–Einstein equation with a radius of 0.42 nm for this anion. The viscosity of the lipid, 1–10 poise, can only account for a 10^2–10^3 decrease in the mobility. Since this is 10^7–10^6 less than the observed decrease of $\sim 10^9$, diffusive mobility in the membrane is not limiting, and there must be a large barrier ($\sim$9 kcal mol^{-1}) to $TPhB^-$ crossing of the membrane or of the membrane-water interface. The barrier also explains why only a weak aqueous ion depletion effect is observed in the steady state of G_{dk}. The effect of stirring is small at times $\sim$ 10 s but can become severe at longer times. The diffusion limited current can be estimated by the method of Lauger et al. (1981) to be $\sim$20–30 pA using the above values. The observed current at 10^{-7} M $TPhB^-$ is $\sim$10 pA at 40 mV. As saturation of conductance sets in, the current can only become less limited by diffusion.

The location of this barrier is of considerable interest. The analysis of transient current responses to voltage steps by Andersen and Fuchs (1975) and by Lauger et al. (1981) places the barrier at the interface. Flewelling and Hubbell (1986*b*) estimate the potential energy or barrier at the center of the membrane due the favorable hydrophobic and electrostatic and unfavorable Born energies to be $\sim$10 kcal/mol ($\sim$430 mV) for $TPhB^-$, sufficient to explain the lower mobility. Unless the potential for $TPhB^-$ is about the same at the interface, this places the barrier at the center of the membrane, contrary to the conclusions of Andersen et al. (1975, 1978) and of Lauger et al. (1981). It is known that Born energies are overestimated by the simple formula and are usually adjusted by arbitrary increases in the ionic radii. Our exponentially varying dielectric produces a smaller Born energy (Raudino and Mauzerall, 1986). The energetics of ions in membranes is not yet resolved.

Membrane potential

A positive inner membrane potential is usually assumed to explain the 10^3–10^4 larger binding constant for negative lipophilic ions than that of similar positively charged ions (Flewelling and Hubbell, 1986*b*). This positive membrane potential subtracts from the energy barrier for $TPhB^-$ ions crossing the membrane and adds to the energy for $TPhP^+$. It has usually been assigned to oriented ester carbonyl dipoles. In addition to calculating the potential due to the lipophilic ion lattice, our models allow a calculation of membrane potential due to the oriented lattice of ester carbonyls, as well as the phosphatidycholine head groups of the membrane. Structural studies of lipid bilayers indicate that one of the carbonyl dipoles is oriented at $\sim$45° with the carbon directed toward the inside of the bilayer, and the other carbonyl is about parallel to the membrane-water interface (Zaccai et al., 1979). Since the dipole moment of an ester carbonyl is 1.4 ± 0.4 Debye (1 Debye = 3.4×10^{-21} C nm), the lipid surface density is 1.47 nm^{-2}, and since the distance between the carbon and oxygen normal to the interface is 0.087 nm, there is a positive dipole potential in the hydrocarbon core of the membrane. Using the two-dielectric model with $\epsilon = 25$, we calculate a carbonyl dipole potential of $\sim$110 mV in the center of the membrane by summing the potential from each side. Using the exponential-dielectric model and the same parameters, the carbonyl dipole potential is $\sim$50 mV and $\sim$105 mV using the exponential-core model with a 4-nm core. The smaller value calculated by the exponential-dielectric model is due to the exponential dielectric extending to the center of the membrane rather than spanning just the ester head group region. These values are probably more realistic than the 250 mV previously calculated by Flewelling and Hubbell (1986*b*) using a dielectric constant of 2. Our values for the dipole potential are less than the 200 mV needed to explain the charge asymmetry of hydrophobic ion binding. Moreover, these potentials are calculated at the center of the membrane, and they are >10-fold smaller at the hydrophobic ion binding site.

It has been suggested (Bauerle and Seelig, 1991; Scherer and Seelig, 1989) that small conformation changes in the phosphatidylcholine head groups may account for the differences in the binding energies of positive and negative lipophilic ions. Our calculations show that small movements of the charged moieties in the phosphatidylcholine head groups can produce a significant potential inside the membrane. The exponential dielectric calculation indicates that the potential *at the lipophilic ion lattice depth* is $\sim$20 mV if the perpendicular component of the positive, choline end of the dipole ($\rho = 1.5\ nm^{-2}$) is only 0.05 nm, and $\sim$40 mV if it is 0.1 nm inside the membrane. The exponential-core model shows that the potential at this site in the membrane is $\sim$90 and $\sim$180 mV, respectively, for the same distances. The asymmetry in the conduction between positive and negative lipophilic ions can be explained if the movement of the positive choline charge toward the membrane center is easier, for electrostatic and/or lipid conformational reasons, than is the movement of the negative phosphate charge. Although this movement is electrostatically disfavored in a neutral membrane (Raudino and Mauzerall, 1986), the presence of the $TPhB^-$ ion lattice may make it more favorable, i.e., the lipid orientates to accommodate the charged ion. If this hypothesis is correct, then lipids with different polar head groups should have differing partition coefficients for anions and cations. In fact, the ratio of β (dipicrylamine$^-$) to β (P-valinomycin K^+) for oleyl phosphatidyl ethanolamine is only one-tenth that for oleyl phosphatidyl choline and that of mono-olein is only a hundredth that of the choline derivative (Benz and Gisin, 1978).

Gawrisch et al. (1992) have shown that a carbonyl group is unnecessary to form a positive potential in a lipid bilayer. They propose that oriented water molecules cause this potential. However, both the ester and ether lipids they used were phosphatidylcholines. Other factors also have been considered, such as the difference in the free energies of transfer between these ions, which have been estimated to be <1 kcal mol^{-1} (Kim, 1978), and so do not significantly contribute to the observed differences in binding. We conclude that an intriguing cooperative movement of the choline head group and the hydrophobic ions may explain the asymmetry in ion binding to the zwitterionic membranes.

CONCLUSIONS

The saturation data of the dark conductance of $TPhB^-$ and $TPhP^+$ through a lipid bilayer is well fit by both a two-dielectric and an exponential-dielectric model for the electrostatic calculation of the space charge formed in the bilayer by the hydrophobic ions. The potentials calculated for the photoformed lattice of $MgOEP^+$ indicate that it can only partially account for the photogating of hydrophobic ion conductances across the membrane by cancellation of space charge. These electrostatic models allow a determination of the distances inside the membrane for a variety of hydrophobic ions and explain both the observations reported here and the conductance saturation reported previously (LeBlanc, 1969; Andersen et al., 1978; Lauger et al., 1981; Flewelling and Hubbell, 1986*a*, *b*). The fluid nature of the membrane makes this a dynamic system. Thus, values of a, b, and ϵ_1 used to fit the data should be considered mean values of distributions. The calculations underscore the importance of discrete charges in determining the potentials within membranes. They also bring out the importance of electrostatic shielding by a variable dielectric region. This effect is lost in the usual image calculation for two dielectrics because the variable region is reduced to a mathematical point or surface. The finite variable dielectric region of real interfaces causes an electrostatic shielding that may have important consequences in biological systems. This analytical solution to a spatially variable dielectric is also an excellent model for dielectric saturation close to ions with large electrostatic fields.

Since photocharging occurs inside the membrane on the nanosecond time scale, the transients of ion transport can be examined with minimal capacitative problems associated with the charge and voltage pulse techniques. These fast transients are important because they contain kinetic information from which the mechanism of ion transport across membranes can be deduced. The kinetics of these lipophilic ions and their implications on the mechanism for ions crossing the membrane are discussed in the companion article (Drain and Mauzerall, 1992).

This photo and redox-gated system is a working example of a molecular ionic photo or redox transistor and is a realistic nanoelectric device (Drain and Mauzerall, 1990).

APPENDIX 1

Two-dielectric model

The method of images in electrostatics (Harnwell, 1949) is used to calculate the potential inside the membrane by summing the contributions from each ion in square lattices of both the lipophilic ion in the membrane and its counter ion in the aqueous solution. The potential, V, for a single charge pair along z, perpendicular to the membrane-water interface at the origin, Fig. 1, is:

$$V = (q/4\pi\epsilon_0\epsilon_1)\{[(z+e)^2 + r^2]^{-1/2} + (\epsilon_1 - \epsilon_2)/(\epsilon_1 + \epsilon_2)[(z-e)^2 + r^2]^{-1/2} - 2\epsilon_1/(\epsilon_1 + \epsilon_2)[(z-f)^2 + r^2]^{-1/2}\}, \quad \text{(A1-1)}$$

where ϵ_0 is the vacuum permittivity, ϵ_1 and ϵ_2 are the dielectric constants in the membrane and aqueous phases, $r^2 = x^2 + y^2$, $e = a - (d_m/2)$ is the distance of the hydrophobic ion from the surface of the membrane in this calculation (see Fig. 1), and $f = b + (d_m/2)$ is the counter ion distance from the membrane surface in the aqueous phase. The potential along an ion pair axis, z, of the two-dimensional square lattice of charge is obtained by the following algorithm that sums (I, J) over the $4N^2$ lattice points.

```
R=E2/E1                 !ratio of the dielectric constants ε2/ε1
F1=(1-R)/(1+R)          !second dielectric weighting term
F2=2/(1+R)              !third dielectric weighting term
F3=((Z+E)*(Z+E))*P      !P is the charge density of hydrophobic
                        ions = ρ
F4=((Z-E)*(Z-E))*P      !these terms are normalized to d=P^-1/2
F5=((Z-F)*(Z-F))*P
FOR I=1 TO N            !scans through the lattice I,J
FOR J=0 TO N            !omit the potential of the pair along the axis
                        of the calculated potential; it is contained in
                        the binding constant, β of Eq. 4.
Q=I*I+J*J
M=M+1/SQR(F3+Q) + F1/SQR(F4+Q) + F2/SQR(F5+Q)
NEXT J
NEXT I
M=M*(4/E1)              !completes the square lattice by symmetry
U=M*56*P^1/2            !energy normalized to kT for a negative test
                        charge
                        !Coulomb radius in vacuo: rc=q^2/4πε0kT =
                        56 nm
                        !P^1/2=ρ^1/2=d^-1 from the normalization of
                        distances
V=M*1.44*P^1/2          !potential q/4πε0 = 1.44 V nm
```

Where Z is the position of the test charge along the perpendicular axis at the chosen lattice point, P is the charge density (nm^{-2}), $4N^2$ is the total number of lattice points, E is the location from the surface of the hydrophobic ion lattice in the bilayer, and F is the location of the counter ion in the aqueous phase. The z axis is chosen along the charge pair because it is the minimum in the potential for a negative ion traversing the membrane. The partition coefficient, β, in the implicit Eq. 1 includes the self energy of the "missing" dipole. A plot of $1/M$ versus $1/N$ for several values of N yields a straight line allowing extrapolation to the infinite lattice and indicates that N = 100 (a 200 × 200 = 4×10^4 site lattice) gives 98.9% of the value for the infinite lattice. The "M" at a lattice site with $\epsilon_2 = \epsilon_1$ agrees with that calculated for a square lattice of dipoles, 9.1 (Topping, 1927), proving our summation algo-

rithm is correct. The curves used to fit the data in Figs. 2 and 3 are calculated by inverting the implicit Eq. 1, fixing ρ_{TPhB^-} and β, and calculating the bulk concentration. Note that in this calculation, the physical size of the lattice varies as $\rho^{-1/2}$. Thus, at large ρ one must determine that $N(\rho)^{-1/2} \gg d_m$ to avoid lattice edge effects. Taking N as 100 satisfies this requirement. Using "HP-Basic" on an HP-340 computer, this calculation of a 200 × 200 lattice takes ~2 s for a given charge density. The potential profile of this lattice across the membrane is calculated by varying z from 0 to the center of the membrane and adding the potential of the lattice at the other interface by reflection. The contribution from the ester group carbonyls is calculated in the same manner but using a real, not a point dipole, with charge = 0.203 C (cos 45°) to obtain the perpendicular component of the dipole. Eq. A1-1 must be modified since both charges are in ϵ_1:

$$V = (q/4\pi\epsilon_0\epsilon_1)\{[(z+e)^2 + r^2]^{-1/2} + (\epsilon_1 - \epsilon_2)/(\epsilon_1 + \epsilon_2) \times [((z-e)^2 + r^2)^{-1/2} - ((z+f)^2 + r^2)^{-1/2}] - (\epsilon_1 - \epsilon_2)/(\epsilon_1 + \epsilon_2)[(z-f)^2 + r^2]^{-1/2}\}. \quad \text{(A1-2)}$$

APPENDIX 2

Exponential-dielectric model

The following treatment of V considers a variable dielectric. From Maxwell's equations for space outside the fixed charges,

$$\text{div}\,(\epsilon\ \text{grad}\ V) = 0. \quad \text{(A2-1)}$$

For a constant ϵ this leads to Laplace's equation, $\nabla^2 V = 0$. It has been shown (Raudino and Mauzerall, 1986) that an exponential distribution of ϵ along one axis also allows analytical solutions of Eq. A2-1.

$$\epsilon_z = \epsilon_c \exp(hz). \quad \text{(A2-2)}$$

This is an appropriate model for a lipid bilayer. The ϵ increases from the membrane interior to the interface along an axis (z) perpendicular to the membrane and is constant along the x and y axis for a given ϵ on the z axis, i.e., $\epsilon_x = \epsilon_y = \epsilon_z$, i.e., the dielectric is inhomogeneous but isotropic. Substituting the variable $S = \epsilon_z^{1/2} V$, Eq. A2-1 reduces to the Poisson equation (Raudino and Mauzerall, 1986).

$$\nabla^2 S - (h^2/4)S = 0. \quad \text{(A2-3)}$$

The potential for a point charge q at a on the z axis is found to be:

$$V = (q/\epsilon_0 r)\exp\{-h[r + (z-c)]/2\}, \quad \text{(A2-4)}$$

where $r = [x^2 + y^2 + (z-a)^2]^{1/2}$. This allows for a difference in origins of the charge $(z-a)$ term and the dielectric distribution $(z-c)$ term. Note that the result is a Coulomb potential screened by the variable dielectric. We can now use this inhomogeneous potential in our summation program, Appendix 1, to calculate the potential from a square lattice of finite dipoles in a material of exponentially varying "dielectric constant" (Fig. 4). This potential automatically accounts for variable dielectric polarization. In the case of discontinuous dielectrics, this polarization is usually estimated by the method of images, as we did before (Appendix 1) (Drain et al., 1989). This model is still discontinuous at the membrane-water interface, but there ϵ is large, so we ignore these small effects (Raudino and Mauzerall, 1986).

Exponential-core model

In this model, we have three regions: the polar region of exponentially decreasing dielectric, a nonpolar core region of low dielectric, and the opposite polar region of exponentially increasing dielectric (Fig. 5 *A*). Because of the membrane and charge symmetry, we place the origin of the z axis at the center of the membrane. The ion lattices are at a and the counter ion lattices at b, and their locations are discussed in the text. We estimate the potential in the core region by fitting at the boundary, $z = c$. The potential in the constant, high dielectric water region could also be calculated by a similar continuation. In this nomenclature, c and $-c$ are the boundaries of the low dielectric region, $d_m/2$ the half thicknesses of the membrane, and the ion lattices are at a and b. The potentials must match at the boundaries c and $-c$. Using the same definition for r:

$$c < z \le d_m/2 \quad V = q/4\pi\epsilon_0\epsilon_c r[\exp(-hr/2)/\exp(h(z-c)/2)] \quad \text{(A2-5)}$$

$$-c < z \le c \quad V = qs/4\pi\epsilon_0\epsilon_c r \quad \text{(A2-6)}$$

$$-d_m/2 < z \le -c \quad V = qt/4\pi\epsilon_0\epsilon_c r[\exp(-hr/2)/\exp(h(-z-c)/2)] \quad \text{(A2-7)}$$

where

$$s = \exp\{(-h/2)[x^2 + y^2 + (c-a)^2]^{1/2}\}/[x^2 + y^2 + (c-a)^2]^{1/2}$$

and

$$t = \exp\{h/2[x^2 + y^2 + (-c-a)^2]^{1/2}\}$$

There are similar equations for the opposite charge at $z = b$. ϵ_c is the dielectric constant in the core region of the membrane.

We thank Dr. Mark Evans at The Rockefeller University for substantial help on the electrostatic problems and Drs. O. S. Andersen and S. McLaughlin for helpful discussions.

This research is supported by the National Institutes of Health grant GM-25693.

Received for publication 24 February 1992 and in final form 20 July 1992.

Note added in proof: Zheng and Vanderkooi (Zheng, C., and G. Vanderkooi. 1992. *Biophys. J.* 63, 935–941) claim that the dipole field inside a lipid bilayer originates in ordered water molecules, since the choline group contributes a negative internal potential. However, they used a lipid crystal structure with the P–N dipole at a fixed 15° angle, positive end outside. They solved a linearized Poisson–Boltzmann equation with a finite difference algorithm on an 86^3 grid of 0.8A cells. Qualitatively, our calculations would agree for this orientation of the choline group. However, they did not allow the P–N axis to move, and thus their conclusion of the contribution from water may well be overstated.

REFERENCES

Andersen, O. S., and M. Fuchs. 1975. Potential energy barriers to ion transport within lipid bilayers. *Biophys. J.* 15:795–830.

Andersen, O. S., A. Finkelstein, I. Katz, and A. Cass. 1976. Effect of phloretin on the permeability of thin lipid membranes. *J. Gen. Physiol.* 67:749–771.

Andersen, O. S., S. Feldberg, H. Nakadomari, S. Levy, and S. McLaughlin. 1978. Electrostatic interactions among hydrophobic ions in lipid bilayer membranes. *Biophys. J.* 21:35–70.

Bauerle, H.-D., and J. Seelig. 1991. Interaction of charged and uncharged calcium channel antagonists with phospholipid membranes. Binding equilibrium, binding enthalpy, and membrane location. *Biochemistry* 30:7203–7211.

Bender, C. J. 1988. Voltammetric studies of ion transfer across model biological membranes. *Chem. Soc. Rev.* 17:317–346.

Benz, R., and B. F. Gisin. 1978. Influence of membrane structure on ion transport through lipid bilayer membranes. *J. Membr. Biol.* 40:293–314.

Braun, H. P. 1987. The transport of hydrophobic ions across lipid bilayers. *Biochim. Biophys. Acta.* 903:292–302.

Cevc, G. 1990. Membrane electrostatics. *Biochim. Biophys. Acta.* 1031:311–382.

Cherry, R. J., K. Hsu, and D. Chapman. 1972. Polarized absorption spectroscopy of chlorophyll-lipid membranes. *Biochim. Biophys. Acta.* 267:512–527.

Drain, C. M., and D. Mauzerall. 1990. An example of a working molecular charge sensitive ion conductor. *Bioelectrochem. Bioenerg.* 24:263–268.

Drain, C. M., and D. Mauzerall. 1992. Photogating of ionic currents across the lipid bilayer: hydrophobic ion conductance by an ion chain mechanism. *Biophys. J.* 63:1556–1563.

Drain, C. M., B. Christensen, and D. Mauzerall. 1989. Photogating of ionic currents across the lipid bilayer. *Proc. Natl. Acad. Sci. USA.* 86:6959–6962.

Ellena, J. F., R. N. Dominey, J. S. Archer, Z.-C. Xu, and D. S. Cafiso. 1987. Localization of hydrophobic ions in phospholipid bilayers using ^{1}H nuclear Overhauser effect spectroscopy. *Biochemistry* 26:4584–4592.

Flewelling, R. F., and W. L. Hubbell. 1986*a*. Hydrophobic ion interactions with membranes: thermodynamic analysis of tetraphenylphosphonium binding to vesicles. *Biophys. J.* 49:531–540.

Flewelling, R. F., and W. L. Hubbell. 1986*b*. The membrane dipole potential in a total membrane potential model: applications to hydrophobic ion interactions with membranes. *Biophys. J.* 49:541–552.

Gawrisch, K., D. Ruston, J. Zimmerberg, V. A. Parsegian, R. P. Rand, and N. Fuller. 1992. Membrane dipole potentials, hydration forces, and the ordering of water at membrane surfaces. *Biophys. J.* 61:1213–1223.

Geske, D. H. 1959. The electrooxidation of the tetraphenylborate ion: an example of a secondary chemical reaction following the primary electrode process. *J. Phys. Chem.* 63:1062–1070.

Harnwell, G. P. 1949. Principles of Electricity and Electromagnetism. McGraw-Hill, New York. 670 pp.

Hille, B. 1984. Ion Channels of Excitable Membranes. Sinauer, Sunderland, MA. 426 pp.

Hong, F., and D. Mauzerall. 1976. Tunable voltage clamp method: application to photoelectric effect in pigmented bilayer lipid membranes. *J. Electrochem. Soc.* 123:1317–1324.

Honig, B. H., W. L. Hubbell, and R. F. Flewelling. 1986. Electrostatic interactions in membranes and proteins. *Annu. Rev. Biophys. Biophys. Chem.* 15:163–193.

Ilani, A., and D. Mauzerall. 1981. The potential span of photoredox reactions of porphyrins and chlorophyll at the lipid bilayer-water interface. *Biophys. J.* 35:79–92.

Ilani, A., T. M. Liu, and D. Mauzerall. 1985. The effect of oxygen on the amplitude of photodriven electron transfer across the lipid bilayer-water interface. *Biophys. J.* 47:679–684.

Jackson, J. D. 1975. Classical Electrodynamics. 2nd ed. John Wiley and Sons, New York. 848 pp.

Kim, J. I. 1978. Preferential solvation of single ions. A critical study of the Ph_4AsPh_4B assumption for single ion thermodynamics in amphiprotic and dipolar-aprotic solvents. *J. Am. Chem. Soc.* 82:191–199.

Kleijn, L. J., and W. B. Bruner. 1983. The influence of hydrophobic ions and dipolar molecules on the electrostatic barrier in biomembranes. *J. Theor. Biol.* 100:139–152.

Lauger, P., R. Benz, G. Stark, E. Bamberg, P. C. Jordan, A. Fahr, and W. Brock. 1981. Relaxation studies of ion transport systems in lipid bilayer membranes. *Q. Rev. Biophys.* 14:513–598.

LeBlanc, O. H. 1969. Tetraphenylborate conductance through lipid bilayer membranes. *Biochim. Biophys. Acta.* 193:350–360.

McLaughlin, S. 1977. Electrostatic potentials at membrane-solution interfaces. *Curr. Top. Membr. Transp.* 9:71–144.

McLaughlin, S. 1989. The electrostatic properties of membranes. *Annu. Rev. Biophys. Biophys. Chem.* 18:113–136.

Neumcke, B., and P. Lauger. 1969. Nonlinear electrical effects in lipid bilayer membranes II. Integration of the generalized Nernst-Planck equations. *Biophys. J.* 9:1160–1170.

Neumcke, B., and P. Lauger. 1970. Space charge-limited conductance in lipid bilayer membranes. *J. Membr. Biol.* 3:54–66.

Ogawa, M. Y., and D. Mauzerall. 1988. Evidence for photoinduced charge transfer between metalloporphyrins at the lipid bilayer-water interface. *Biophys. J.* 53:512*a*. (Abstr.)

Parsegian, A. 1969. Energy of an ion crossing a low dielectric membrane: solutions to four relevant electrostatic problems. *Nature (Lond.).* 221:844–846.

Raudino, A., and D. Mauzerall. 1986. Dielectric properties of the polar head group region of zwitterionic lipid bilayers. *Biophys. J.* 50:441–449.

Ricchelli, F., G. Gori, S. Gobbo, and M. Tronchin. 1991. Liposomes as models to study the distribution of porphyrins in cell membranes. *Biophys. Biochim. Acta.* 1065:42–48.

Schere, P. G., and J. Seelig. 1989. Electric charge effects on phospholipid head groups. Phosphatidylcholine in mixtures with cationic and anionic amphiphiles. *Biochemistry* 28:7720–7728.

Simon, S. A., and T. J. McIntosh. 1986. Depth of water penetration into lipid bilayers. *Methods Enzymol.* 127:511–521.

Skinner, J. F., and R. M. Fuoss. 1964. Conductance of triisoamylbutylammonium and tetraphenylboride ion in water at 25°. *J. Phys. Chem.* 68:1882–1885.

Smith, J. C., S. Chandrasekaran, and D. Gill. 1992. NMR studies of the localizations assumed by lipophilic ions in small unilamellar 1,2-dimyristoyl-sn-glycero-3-phosphocholine vesicles. *Biophys. J.* 61: 240*a*. (Abstr.)

Topping, J. 1927. On the mutual potential energy of a plane network of doublets. *Proc. R. Soc. Lond. Ser. A* 114:67–72.

Tsien, R. Y., and S. B. Hladky. 1982. Ion repulsion within membranes. *Biophys. J.* 39:49–56.

Woodle, M., and D. Mauzerall. 1986. Photoinitiated ion movements in bilayer membranes containing magnesium octaethylporphyrin. *Biophys. J.* 50:431–439.

Woodle, M., J. W. Zhang, and D. Mauzerall. 1987. Kinetics of charge transfer at the lipid bilayer-water interface on the nanosecond time scale. *Biophys. J.* 52:577–586.

Zaccai, G., G. Buldt, A. Seelig, and J. Seelig. 1979. Neutron diffraction studies on phosphatidylcholine model membranes. II. Chain conformation and segmental disorder. *J. Mol. Biol.* 134:693–706.